Article:
Mahmood, I, Martinez-Hernandez, U and Dehghani-Sanij, AA (2020) A model identification approach to quantify impact of whole-body vertical vibrations on limb compliant dynamics and walking stability. Medical Engineering & Physics, 80. pp. 8-17. ISSN 1350-4533

https://doi.org/10.1016/j.medengphy.2020.04.005

A model identification approach to quantify whole-body vertical vibrations impact on limb compliant dynamics and walking stability

Imran Mahmood[1], Uriel Martinez-Hernandez[2], Abbas A. Dehghani-Sanij[1]

[1]Institute of Design, Robotics, and Optimisation, School of Mechanical Engineering

University of Leeds, Leeds, United Kingdom

[2]Department of Electronics and Electrical Engineering, Faculty of Engineering and Design,

University of Bath, Bath, United Kingdom

Submitting for Original Article

Corresponding Author

Imran Mahmood

School of Mechanical Engineering

The University of Leeds,

Leeds, LS2 9JT, United Kingdom

Email: mnim@leeds.ac.uk; imran.mahmood@uet.edu.pk

Phone +4407589658714

List of Abbreviations

AFO	Ankle-foot orthosis
BoS	Base of support
CoM	Center of mass
CNS	Central Nervous system
DR	Damping Ratio
DRT	Dorsiflexion resistive torque
DRR	Dorsiflexion range-of-motion restriction
DPRT	Dorsi-plantarflexion resistive torques
DPRR	Dorsi-plantarflexion range-of-motion restrictions
PC1	First principal component
GM(s)	Gain Margin(s)
HS	Heel Strike
IMU	Inertial Measurement Unit
MP	Minimal phase
NMP	Non-minimum phase
N&B	Nyquist and Bode
PM(s)	Phase Margin(s)
PCA	Principal component analysis
ROM	Range of motion
RMS	root-mean-square
SM	spring-mass
SMD	spring-mass-damper
TF(s)	Transfer function(s)
TO	Toe off
WBV(s)	Whole body vibrations

Highlights:

- This study introduces methods to quantify vertical limb dynamics while walking.
- A model identification approach is proposed to quantify lower limb compliant dynamics.
- Linear control theory is applied to analyse the effect of vertical loading impacts on stability.
- Proposed methods are applied to investigate the structural impacts of wearable devices.
- Our methods show that a wearable orthosis has significant effect on the limbs' vertical dynamics.

Abstract

Extensive research is ongoing in the field of orthoses/exoskeleton design for efficient lower limbs assistance. However, despite wearable devices reported to improve lower limb mobility, their structural impacts on whole-body vertical dynamics have not been investigated. This study introduced a model identification approach and frequency domain analysis to quantify the impacts of orthosis-generated vibrations on limb stability and contractile dynamics. Experiments were recorded in the motion capture lab using 11 unimpaired subjects by wearing an adjustable ankle–foot orthosis (AFO). The lower limb musculoskeletal structure was identified as spring-mass (SM) and spring-mass-damper (SMD) based compliant models using the whole-body centre-of-mass acceleration data. Furthermore, Nyquist and Bode methods were implemented to quantify stabilities resulting from vertical impacts. Our results illustrated a significant decrease ($p < 0.05$) in lower limb contractile properties by wearing AFO compared with a normal walk. Also, stability margins quantified by wearing AFO illustrated a significant variance in terms of gain-margins ($p < 0.05$) for both loading and unloading phases whereas phase-margins decreased ($p < 0.05$) only for the respective unloading phases. The methods introduced here provide evidence that wearable orthoses significantly affect lower limb vertical dynamics and should be considered when evaluating orthosis/prosthesis/exoskeleton effectiveness.

Keywords: ankle–foot orthosis, limb contractile properties, dynamic stability, gait, vertical impacts, loading and unloading phases, wearable devices

1. Introduction

People with growing age and/or neuromuscular impairments tend to avoid bipedal activities because of fear of falling [1]. Clinically, a range of lower limb orthoses or exoskeletons is recommended for assistance or rehabilitation [2]. Intensive research studies are ongoing to make these devices portable, lightweight and stronger [3]. Most of the commercially available orthoses/exoskeletons are made of the metallic structure strapped rigidly to the lower limbs for efficient power transmission. Earlier studies have reported that the vertical impact forces generated because of inertial changes at the lower extremity (ankle–foot) are two to three times of the body weight and resultant shock waves are considered as one of the major reasons for worsening joint diseases and neuromuscular injuries [4, 5]. However, their effects on gait dynamic stability and lower limb contractual properties have not been reported in view of wearable devices. Lower-limbs contractile properties are being used to simulate walking dynamics in terms of spring-mass system [6-8]. Such models are also built in portable motion monitoring devices such as inertial measurement units [9] to understand limb compliant dynamics.

Considering prior modelling approaches, studies have developed various bipedal models to simulate lower limb vertical dynamics to investigate limb contractile properties and neuromotor control aspects. These include spring-mass [7, 10, 11] and spring-mass-damper [6, 8, 12] based inverted pendulum models in which model parameters are adjusted to get a model output equivalent to the ground reaction force (GRF) data collected experimentally from human subjects. These approaches use rigid body elements (e.g., spring, mass and damper models) that underestimate the actual impact dynamics in the lower limbs during weight loading and unloading gait phases. During these phases, a rate of deceleration or acceleration illustrates highly transient features and also acts as somatosensory feedback to actuate leg muscles [13-15]. Alternatively, a few studies also employ a general second-order

119 underdamped system in which model parameters (natural frequency, damping ratio) are
120 estimated using time series data collected from human subjects [16, 17]. These fixed-order
121 empirical models also underrate limb vertical dynamics to mimic actual gait transients which
122 illustrate sinusoidal patterns. Furthermore, the efficiency of the best-fit models has not been
123 reported in either of the mentioned modelling approaches. Because of these limitations, lower
124 limb contractile properties are previously reported with large variations [18]. A critical need
125 remains to validate previously reported lower limb vertical dynamics by applying methods
126 that will address the highlighted discrepancies.

127 Recent studies also apply whole-body vertical vibrations/impact forces as a rehabilitation tool
128 to recover from chronic ankle instabilities, ankle sprains and muscular or neural deficits [19-
129 21]. Oppositely, a range of heel pads is also reported in prior studies to damp the vertical
130 loading impacts [22, 23]. Previously, the effectiveness of these rehabilitation techniques on
131 gait dynamic stability is reported to assess in anterior-posterior and medial-lateral directions
132 [24, 25] but lacked to quantify in the vertical direction despite the vertical GRFs having
133 maximum magnitudes and rate of variations. That may be because of the methodological and
134 or analytical limitations in existing techniques used to simulate limb vertical dynamics.

135 This study proposes methods of identifying lower limb compliant models directly from the
136 experimental data. From the engineering control theory, Nyquist and Bode (N&B) methods
137 are implemented to analyse the effect of compliant dynamics on walking stability. More
138 recent studies employed these techniques for gait dynamic stability assessments in the
139 forward direction of motion [26-28]. These methods are applicable to quantify gait
140 stability/instability in all three anatomical directions, hence, overcome the limitations of
141 previously reported assessments [24, 29] which were reported in the anterior-posterior and
142 medial-lateral directions (deficient to quantify the impact of vertical forces). This study
143 extends the work done previously by considering vertical loading impacts while performing a

level ground walk. Furthermore, these methods are applied to investigate wearable ankle–foot orthosis (AFO) impacts on the vertical limb dynamics for a range of clinically applied adjustments.

2. Materials and Methods

2.1 Experimental protocol and setup

A total of 11 healthy subjects (aged 30±1 yrs, weight 74±3 kg and height 1.72±2.5 m) were included in this study. The subjects were inducted with no prior history of neurological or neuromuscular impairments. Each subject signed an informed consent form. The experimental protocol was approved by the institutional ethical review board at the University of Leeds.

An adjustable ankle–foot orthosis was designed to induce perturbations into the ankle joint in the sagittal plane following earlier studies [30, 31]. The AFO was made with metallic (aluminium) shank and carbon-fibre foot parts embedded with an adjustable Ultraflex ankle–foot joint [32] as shown in **Figure 1(a)**. The AFO was tuneable to a range of clinical stiffness and a range of motions (ROMs; ±67.8 Nm and ±40°) both in dorsiflexion and plantarflexion directions. The simulated ankle–foot restrictions and their operating ranges are summarised in **Table 1**. The AFO restrictions were implemented following prior studies [30, 33] in which various gait-related aspects were investigated by applying restrictions to the healthy subjects ankle-foot joint. Clinically, these restrictions are tuned using AFO to treat ankle-foot deficiencies such as foot drop, Charcot-Marie tooth etc. A total of 26 reflective markers were attached to the body at lower limbs. The placement of the markers was followed from Visual-3D help document [34] as illustrated in Figure A1 (Appendix A). The subjects were asked to get familiar with the AFO by wearing it on an eight-metre walkway, and then the trials were recorded in a motion capture lab using 12 cameras (Qualisys software and Oqus cameras) and

two force plates (AMTI BP400600-2000) at 1 kHz and 400 Hz, respectively. The trials were recorded first at normal speed barefoot, then wearing AFO (free mode) and applying the aforementioned restrictions. Prior to recording the experiments, each participant was asked to perform a few trials to get familiar with his preferred normal pace and to ensure this pace in all walking conditions. The preferred walking speed trials were recorded following previously reported similar studies [35-37]. A total of five trials were recorded per subject per walking condition.

Table 1 here

Figure 1 here

2.2 Data processing

The lower-limb joint angles and moments were computed using Visual3D motion analysis software (C-Motion Inc., Germantown, MD) and filtered at 6 Hz using fourth-order Butterworth. The ankle and knee joint angles and moments are illustrated in **Figure 1(b–e)**. The vertical GRF raw data was exported to MATLAB 2017a and normalised with individual subject body weight. The resultant signals present whole-body CoM-acceleration (i.e. GRF/mass) which were further processed into two steps. Firstly, the finite difference algorithm [38] was implemented using Eq. 1 to determine the rate of change in the body's CoM-acceleration ('$\dot{a}$' unit m/s^3). The resultant waveforms were filtered using Butterworth fourth order filter at 18Hz and illustrated in **Figure 2(a) –** named as actual CoM-oscillations (i.e. before rectification).

$$\dot{a} = (a_2 - a_1)/(t_2 - t_1) \quad (1)$$

where a_2, a_1 are two consecutive samples of CoM-acceleration and t_2, t_1 are respective time instants. Secondly, the root-mean-square (RMS) of the aforementioned CoM-oscillations

191 ($\dot{a}_{rms}$) was computed using Eq. 2. The RMS of CoM-oscillations was computed following
192 prior similar studies [37, 39, 40] where higher order signals (derivative) were reported to be
193 rectified in-order to analyse or characterise important features in the frequency domain.
194 Likewise, in the current study, a frequency domain stability analysis was performed to the
195 RMS CoM-oscillations as discussed in the subsequent section 2.3.

196 $$\dot{a}_{rms} = \sqrt{(\dot{a}_1)^2 + (\dot{a}_2)^2/2} \quad (2)$$

197 Where $\dot{a}_1$ and $\dot{a}_2$ are the rate-of-change of CoM-acceleration and present two consecutive
198 samples of the actual CoM-oscillations. The RMS CoM-oscillations were time normalised to
199 500 samples (stance phase) and filtered using fourth-order Butterworth filter at 18 Hz. After
200 computing the RMS and filtering the waveforms, the resultant vertical CoM-oscillations are
201 plotted in Figure 2(b). Both the actual and respective RMS waveforms of CoM-oscillations
202 are presented in Figure 2(a) and 2(b) respectively for the normal walking condition. An
203 optimum cut-off frequency for the Butterworth filter is selected applying residual analysis
204 method [41] to the raw waveforms of CoM-oscillations and the order of the filter was
205 confirmed from prior similar studies [42]. The data filtration using fourth order Butterworth
206 at 18Hz removed the noise effectively, however, due to averaging of consecutive samples, the
207 last few samples of the unloading phases illustrated over smoothening in Figure 2(a). To
208 overcome this issue, the whole stance phase (500 samples) was split into two windows of
209 equal lengths. Each window (250 samples) was processed independently while computing
210 RMS and applying filtration. Thus, the windowing of the stance phase eliminates the over
211 smoothening effect and resultant waveforms are illustrated in Figure 2(b). The resultant
212 CoM-oscillations showed oscillatory impulsive responses with decaying magnitudes in
213 loading and rising magnitudes during the respective unloading phases as shown in **Figure**
214 **2(b)**. Observing these responses, window sizes of 150 samples were selected for further

analysis such that the initial 30 percent of the stance from heel contact (HC) present the loading phase and the last 30 percent towards toe-off present the unloading phases [43].

Figure 2 here

The derivative of CoM-acceleration waveforms induced noise in the output data. Furthermore, the variations in the subjects' demographic data (weight, height and foot length) and adaptability towards orthosis restrictions induced artefacts in the output waveforms. These artefacts induce variability and hence nonlinearity in the data. In order to confirm this non-linearity resulted due to demographic variations among the subjects, at first, the PCA was performed using a single subject all trials and the results illustrated that the first principle component (PC1) counted 99% of the variance of the input waveforms. Further, the PCA was applied combined to all eleven subjects' walking trials and results illustrated that the variation explained by PC1 reduced to 90%. Implies, the combined data scatted in other dimensions as well. Thus, the demographic variations among the testing subjects induced non-linearity. The requirement for analysing these oscillatory waveforms applying Nyquist and Bode methods is to be modelled using linear time-invariant models. Following similar applications from prior studies [44, 45], we have implemented principal component analysis (PCA) to reduce the artefacts from repeatedly measured oscillatory waveforms. This technique converts a set of correlated variables into linearly uncorrelated variables called principal components (PCs). For each walking condition, an input data matrix (5 trials x 11 subjects) was used to reduce the variability in the data following an earlier study [46]. The PCs which explained variances >80% were used to reconstruct the linear waveforms. The mean of each subject's five trials was used for further analyses.

2.3 CoM-vibrations modelling and analysis

In the vertical direction, the resultant CoM-oscillations were modelled in time and frequency domains applying two different model identification approaches as illustrated in **Figure 3**. Since vertical GRF vector presents the resultant of whole-body inertial impacts, spring-mass or spring-mass-damper models were used to present the resultant effect of whole limb dynamics. In the first approach, a sum of sinusoidal functions was found the best fit (99±0.5%) to the time series linear waveforms applying curve fitting tools (least square regression) in MATLAB 2017a for both loading and unloading phases (models presented in Appendix – Table A.1). This approach follows the spring-mass system identification, with the assumption damping ratio approaching zero and the body experiencing free vibrations. The time-domain models were converted to the frequency domain by Laplace transformation, also known as transfer function (TF). In the second approach, frequency-domain models were identified directly as the ratio of output to input polynomials using the System Identification Toolbox in MATLAB with criteria of best fit >95% (models presented in Appendix – Table A.1). This approach follows spring-mass-damper (SMD) based model identification with relatively less fit for loading phase waveforms and unable to predict the unloading phase at all. Hence, the second approach was used to quantify contractile properties as a result of loading impacts, including the effect of damping factor.

Figure 3 here

A transfer function presents a system in the frequency domain as a ratio of Laplace of the output to input polynomials. The roots of the denominator of a TF are used to define the stability of a system (i.e., stable if it lies on the left half of the s-plane; otherwise, it is unstable). Furthermore, the modelled TFs can illustrate the non-minimum phase (NMP) systems in which numerator/denominator roots lie on the right half of the s-plane (Figure A2). Based on a study, most of the flexible systems had NMP natures and were found difficult to analyse [47]. We have applied unit impulse inputs to the modelled TFs, which is a

standard control engineering approach to test systems responses in the frequency domain [28] and resultant outputs presented the CoM-oscillations as gain and phase plots in the frequency domain (Figure A3).

2.4 Nyquist and Bode (N&B) stability criteria

The N&B methods present TFs graphically as gain or phase versus logarithmic frequency axes (Figure A3). Both methods are applied alternatively; however, Bode plot is more widely used with its distinct graphical representation for gain and phase plots compared with an equivalent single Nyquist plot. Here, both methods were implemented, and stability margins were confirmed from each other. The Nyquist criteria define relative stabilities in terms of gain and phase margins. It employed Cauchy's theorem with distinct stability cutoffs (i.e., 0 dB gain and $\pm 180° \pm 2k\pi$ phase) with reference of which stability margins are quantified such that the points where gait and phase plots cut respective axis are called cutoff frequencies. At phase cutoff frequency, the difference of gain plot from '0dB axis' measures gain margin (GM), and at gain cutoff frequency, the difference of phase magnitude from '$\pm 180° \pm 2k\pi$ axes' measures as phase margins (PM) as illustrated in Figure A3. The GM and PM quantify the ability of a system to withstand internal or external disturbances. Applying Nyquist and Bode methods, the gait instability refers to how much a person deviates from the point of stability for which the reference thresholds are 0dB gain and $\pm 180°$ phase. A GM quantifies robustness with respect to amplitude, and a PM quantifies the ability to withstand time delays. A system may have one or more GMs and PMs, and among those, the one with the smallest absolute margin would be critical to define the system's stability [48]. The contractile properties define lower-limbs overall compliant dynamics (resultant of muscles activation) such as damping ratio, natural frequency and peak gain. These properties quantify limb impact forces attenuation properties. Previously, these contractile properties were evaluated using resultant ankle moments [16] or vertical GRFs [6, 18]. These properties have

been used to differentiate healthy versus impaired subjects' ability to generate/absorb impact forces. In the current study, the structural impact of a wearable orthosis on the limb compliant dynamics are evaluated using these properties. These properties are defined here using formulae described in control theory texts [49] (Figure A4).

1) Damping Ratio (DR) - The damping ratio is a dimensionless quantity that quantifies the system's ability to attenuate oscillations/vibrations in response to a disturbance. Practically, an underdamped system has $0 < \zeta < 1$, and an undamped system has $\zeta = 0$. A decrease in the damping ratio implies more oscillations resulting from heel contact.

$$\zeta = -\cos(\theta)$$

where 'θ' is the angle from the origin to the pole location.

2) Peak Gain (Mr) - It presents the maximum magnitude in the gain plot. For a normal gait performance, peak gains are required to maintain the range of healthy subject data to provide optimum somatosensory inputs to the neuromotor for balance control.

3) Natural Frequency (ωn) – This presents the frequency of CoM-oscillations, which is used to analyse the response of a system.

$$\omega n = |s|$$

where 's' is pole location. Since the natural frequency of oscillations depends on pole locations, the pole which presents maximum natural frequency is used for analysis.

2.5 Statistical Analysis

Both contractile properties and stability margins were compared statistically using IBM SPSS-V23 software. First, the distribution of data samples in each variable was tested applying the Shapiro–Wilk test and found overall non-normal distributions ($p < 0.05$).

Observing that, a nonparametric Wilcoxon signed-rank test was applied in pairwise. Gait metrics are considered statistically significant if $p < 0.05$. All AFO walking conditions are compared with a normal walk to understand the effect of an orthosis on gait dynamic stability with/without applying restrictions, and all AFO-restricted walking conditions are also compared with an AFO free-mode walk to understand the dynamic response of AFO adjustments.

3. Results

The best models fitted to whole-body vertical vibrations are identified from the coefficient of determinant (R^2) as described in the Appendix (Tables A.2 and A.3). Lower limb contractile dynamics identified from spring-mass models illustrated that the natural frequency (ω_n) of CoM-oscillations decreased ($p < 0.05$) in all AFO walking conditions when compared with both normal and AFO (free-mode) walks as illustrated in **Figure 4** and Table A.3. The only exception was the dorsi-plantar combined resistance (DPRT) condition which illustrated an increase ($p < 0.05$) in frequency. Considering peak gains (Mr), only the dorsiflexion-restricted walking conditions (i.e., moderate restriction [DRT] and severe restriction [DRR]) showed a decrease ($p < 0.05$) in peak gain compared with a normal walk. The best-fit sinusoidal models illustrated undamped response, that is, the damping ratio (ζ) approaches zero in all walking conditions.

Figure 4 here

Considering the second modelling approach (spring-mass-damper system), the natural frequency of CoM-oscillations are in range to that of the first modelling approach. However, the damping ratio reduced the peak gains as shown in **Figure 5** and Table A.4. Both methods illustrated similar patterns with respect to natural frequency and peak gains, that is, the natural frequency decreased compared with the normal and AFO free-mode walks and the

peak gain decreased compared with a normal walk. Overall, SMD models illustrated a low damping ratio (DR) in all walking conditions. The DR increased by wearing AFO in free mode and decreased significantly on applying restriction compared with both normal and AFO free-mode walks.

Figure 5 here

Walking with AFO in its free mode illustrated no difference in loading phase stability margins compared with a normal walk. However, applying restrictions to the ankle–foot joint by tuning AFO (**Figure 6,** Table A.2), all walking restrictions showed a decrease ($p < 0.05$) in GMs during the loading phase compared with a normal walk, and only totally restricted walking conditions (i.e., DPRR, DRR) showed a decrease in GMs ($p < 0.05$) when compared with an AFO free-mode walk. The PMs increased significantly in all AFO restricted walks when compared with an AFO free-mode walk, and no difference was found when compared with a normal walk. During the respective unloading gait transitions (**Figure 7,** Table A.2), moderately restricted walking conditions (i.e., DPRT, DRT) illustrated an increase ($p < 0.05$) in both GMs and PMs when compared with AFO free-mode walk. Comparing with a normal walk, both moderately restricted conditions also illustrated an increase in GMs, however, decreased in the PMs. In comparison, totally restricted walking conditions (i.e., DPRR, DRR) showed a decrease in GMs and an increase in PMs compared with an AFO free-mode walk. However, both of these restricted walking conditions illustrated a decrease in PMs compared with a normal walk.

Figure 6 here

Figure 7 here

Gait spatiotemporal parameters are also evaluated and summarised in Table A.5 (Appendix A). There is no difference found in the walking speed and stride duration while comparing AFO restricted conditions with AFO free-mode walk. However, a normal walk at preferred speed illustrated a significant increase in both parameters when compared with all AFO walking conditions. The initial double limb support time is significantly increased ($p < 0.05$) in all AFO walking conditions compared with a normal walk.

4. Discussion

The goal of this study was to introduce methods for quantifying vertical vibration impacts on walking stability and lower-limb compliant dynamics. These methods are further applied to investigate wearable orthosis structural impacts. Our results illustrated significant variations in the aforementioned gait dynamics with the effect of wearable AFO which was tuned to various clinically applied ranges (**Table 1**). Compared with prior studies [6, 7], this study evaluated lower limb vertical dynamics directly from the experimental GRF data applying system identification approach. The identified models included spring-mass (SM) and spring-mass-damper (SMD) based approaches with predictable best-fit coefficients. In earlier studies, the rigid elements, such as body mass, spring stiffness and damper parameters, are adjusted randomly to achieve the resultant GRF close to the experimental data. These empirical models are speculated to overrate limb compliant dynamics because of either misfit or missing limb dynamics.

Further analysis of both identified models illustrated that the SM model was found the best fit (99%) to the experimental data and offered lesser variations while quantifying stability margins applying Nyquist and Bode methods. However, SM models do not consider the damping factor that is responsible for the decays in transient impacts generated during heel contact, which illustrates a limitation of the SM-based modelling approach. In comparison,

the SMD-based model identification illustrated large standard deviations in stability margins with relatively less fit to the impact loading waveforms (Appendix Table A.6). That follows the Nyquist stability criteria which quantify GM/PM with respect to the reference point (-1,0j), where a large deviation would result if gain or phase magnitudes deviate [48]. These findings illustrate that the gait dynamic stability evaluation is sensitive to the best-fit model and that spring-mass models are more appropriate for such evaluations. However, the consideration of the damping factor makes the SMD model potentially appropriate while quantifying limb compliant dynamics in the vertical direction. Despite SMD models having the damping characteristics of the lower limbs, this approach was not found to be convergent to the respective unloading phase oscillatory waveforms.

Prior studies illustrate that the CoM-oscillations generated during loading and unloading gait phases transmit along the longitudinal direction of the lower limbs [4] and act as somatosensory feedback to control neuromuscular activations [50]. Our results from SMD models illustrated that the variations in peak gain both with/without wearing AFO are in range (30 to 22 dB) to an earlier study [16] where the limb contractile properties are quantified from ankle–foot torque waveforms fitted to a second-order underdamp model. Furthermore, the peak gains quantified here illustrated decreasing trends by applying restrictions to the ankle joint, also reported previously for patients (50 to 39 dB) [16] having reduced ankle motions because of spastic gait. However, both the damping ratio and the natural frequency of CoM-oscillations (impact forces) are far less in our study compared with a prior study. This might be resultant of the empirical-based modelling approach adopted previously without any predictable accuracy of best fit. In another study [18], SMD model based lower limb compliant dynamics is reviewed and has reported large variations in the damping ratio (0.17 to 1.9), whereas our results support lower ranges (0.25±0.006 for a normal walk) of these reported DRs [6, 7]. This study also illustrated a decrease in DR on

applying moderate to severe AFO restrictions. This implies that the leg muscles are stiffed enough against applied restrictions and unable to generate any further moments. This is consistent with prior studies where the ankle and knee joint moments are reported to increase during loading phases and under similar walking conditions [6, 8].

Considering walking stabilities, the loading and unloading phases are of particular importance, during which a maximum push-off is exerted in the leading limb and braking torque is generated in the trailing limb. Previously reported methods [24, 29] used to quantify gait stability in anterior-posterior and medial-lateral directions (e.g. margin-of-stability quantifies CoM w.r.t BoS), however, the current study scaled the gait stability in the vertical direction and filled this gap. Stability margins quantified in this study illustrated unstable responses during both of these two phases. This is consistent with the prior studies where vertical oscillations were reported to deteriorate the lower limb joints performance [4, 5] and various foot insoles were used to damp their effect [22, 23]. Thus, vertical CoM-oscillations induce instability even in a normal walk, however, this instability normally remains tolerable i.e. the margins are small enough to prevent fall as quantified here as GMs and PMs. This instability diminishes as CoM-oscillations decay towards mid-terminal stance during which these oscillations remain relatively steady-state as illustrated in Figure 2(b). Thus, the periodic instability quantified in this study during loading and unloading phases also reinforce the argument of inherent instability in the human gait and regain of stability during single limb support (i.e. mid-terminal stance - during which CoM remains within BoS in the AP direction).

During the impact loading, our results using SM models illustrated a decrease in instability (GMs) by restricting ankle-foot motion through AFO, and no effect was found in terms of PMs (time delay). Because the AFO rigid structure allows less freedom to the ankle-foot movements, hence, subjects adapted wearable device with a reduction in their preferred

walking speed and joints movements, as a result, the vertical CoM-oscillations reduced both in magnitude (peak gains) and GMs during loading. Also, the increase in initial double-limb-support time by wearing AFO illustrated that the subjects emphasized to stay longer on their double limbs during the loading phase in an effort to maintain instability closer to normal thresholds. Our results for the PMs also reflect this outcome with a relative increase in time delays by wearing AFO, though this increase is statistically insignificant. Thus, a neuromotor control illustrates robustness with respect to time delays during loading phases and decreased peak gains and GMs compared with a normal walk. Earlier studies reported that a nominal range of CoM-oscillations is essential as sensory feedback in neuromotor balance control and muscles activations [51]. Our results for the loading phases illustrated that this sensory feedback gets affected in terms of peak gain and GMs by wearing wearable orthosis.

During the respective unloading phases, the instability quantified by GMs increased in both AFO (free mode) and moderately applied restrictions and decreased for severe restrictions. This is because moderately applied resistive torques allow leg muscles to increase their activity against applied restrictions, also illustrated by an increase in ankle and knee moments near push-off (Table A.7), whereas more severe restrictions do not allow ankle–foot motion at all. Overall, wearable AFO illustrated a reduction in PMs (time delays) compared with a normal walk, although the effect size was small. This is consistent with a prior study where very small delays are reported in the activation of leg muscles in response to AFO plantarflexion resistance [30].

The methods introduced in this study provide a proof of concept that wearable devices affect gait vertical dynamics and hence neuromotor control. The whole-body vertical oscillations were modelled here just like the mathematical models used in Visual3D or OpenSim software to compute gait biomechanics. This study involved various data processing and mathematical steps, but also the following limitations of this work have been identified. Firstly, the

455 analysing signals (i.e. vertical GRFs) are experimentally measured using the force plates only
456 for the stance phase, hence, these methods are limited to assess stance phase stability.
457 Secondly, the best fit models (i.e. curve fitting approach) did not consider the damping effect
458 of the lower limbs, hence, the second approach (i.e. system identification) was adopted with
459 relatively less fit (R^2) to define the limb contractile dynamics completely. Lastly, in this
460 study, the CoM-oscillations modelled using the best-fit criteria (i.e. R^2) were resulted in the
461 higher-order frequency domain transfer functions which can be simplified with little
462 compromise in the results.

463 Summarising, an SMD based model identification was found more predictive to quantify
464 limb contractile dynamics, and SM models were determined appropriate to quantify limb
465 dynamic stabilities. Limb contractile dynamics are important to evaluate in a situation like
466 poor neuromuscular sensation or leg paraesthesia in which patients experience serious
467 weight-bearing problems. These methods are helpful in the differential diagnosis of an
468 impaired limb and in the evaluation of rehabilitative measures such as heel pads, assistive
469 orthosis and vibration therapies. A reduced ankle–foot motion simulated here by wearing an
470 AFO also mimics ankle–foot impairments such as Charcot-Marie-Tooth (CMT), foot drop
471 and spastic gait [52] and thus gives insight for stability evaluation in such patients. Further
472 analysis of modelled limb dynamics applying Nyquist criteria provides critical information
473 about limb stability. In the future, we will extend the scope of our research by acquiring the
474 CoM-oscillations data for the swing phase using IMU sensors and applying model reduction
475 techniques to optimise the higher-order models used in this study. Further, these methods will
476 be applied to evaluate the effectiveness of wearable orthosis in patients with lower limb
477 impairments.

478 **Acknowledgements**

The corresponding author would like to thank his PhD scholarship sponsor, University of Engineering and Technology, Lahore, Pakistan. The authors would like to thank all the participants and lab facility at the University of Leeds.

Conflicts of Interest: None

Funding: None

Ethical Approval: Faculty Research Ethics Committee (MEEC FREC) University of Leeds (Ref. MEEC 15-050)

References

[1] Lugade V, Kaufman K. Center of pressure trajectory during gait: A comparison of four foot positions. Gait & Posture. 2014;40:719-22.
[2] Houx L, Lempereur M, Rémy-Néris O, Brochard S. Threshold of equinus which alters biomechanical gait parameters in children. Gait & Posture. 2013;38:582-9.
[3] Herr H. Exoskeletons and orthoses: classification, design challenges and future directions. Journal of NeuroEngineering and Rehabilitation. 2009;6:21.
[4] Chi K-J, Schmitt D. Mechanical energy and effective foot mass during impact loading of walking and running. Journal of Biomechanics. 2005;38:1387-95.
[5] Wakeling JM, Liphardt A-M, Nigg BM. Muscle activity reduces soft-tissue resonance at heel-strike during walking. Journal of biomechanics. 2003;36:1761-9.
[6] Hong H, Kim S, Kim C, Lee S, Park S. Spring-like gait mechanics observed during walking in both young and older adults. Journal of biomechanics. 2013;46:77-82.
[7] Lim H, Park S. Kinematics of lower limbs during walking are emulated by springy walking model with a compliantly connected, off-centered curvy foot. Journal of Biomechanics. 2018;71:119-26.
[8] Kim S, Park S. Leg stiffness increases with speed to modulate gait frequency and propulsion energy. Journal of Biomechanics. 2011;44:1253-8.
[9] Hamacher D, Hamacher D, Singh NB, Taylor WR, Schega L. Towards the assessment of local dynamic stability of level-grounded walking in an older population. Medical Engineering & Physics. 2015;37:1152-5.
[10] Geyer H, Seyfarth A, Blickhan R. Compliant leg behaviour explains basic dynamics of walking and running. Proceedings of the Royal Society B: Biological Sciences. 2006;273:2861-7.
[11] Ryu HX, Park S. Estimation of unmeasured ground reaction force data based on the oscillatory characteristics of the center of mass during human walking. Journal of Biomechanics. 2018;71:135-43.
[12] Lee M, Kim S, Park S. Resonance-based oscillations could describe human gait mechanics under various loading conditions. Journal of Biomechanics. 2014;47:319-22.
[13] Allen JL, Ting LH. Why Is Neuromechanical Modeling of Balance and Locomotion So Hard? In: Prilutsky BI, Edwards DH, editors. Neuromechanical Modeling of Posture and Locomotion. New York, NY: Springer New York; 2016. p. 197-223.

[14] Graham DF, Carty CP, Lloyd DG, Barrett RS. Muscle contributions to the acceleration of the whole body centre of mass during recovery from forward loss of balance by stepping in young and older adults. PLOS ONE. 2017;12:e0185564.
[15] La Scaleia V, Ivanenko YP, Zelik KE, Lacquaniti F. Spinal motor outputs during step-to-step transitions of diverse human gaits. Frontiers in Human Neuroscience. 2014;8:305.
[16] Hidler JM, Harvey RL, Rymer WZ. Frequency Response Characteristics of Ankle Plantar Flexors in Humans Following Spinal Cord Injury: Relation to Degree of Spasticity. Annals of Biomedical Engineering. 2002;30:969-81.
[17] Hur P, Duiser BA, Salapaka SM, Hsiao-Wecksler ET. Measuring Robustness of the Postural Control System to a Mild Impulsive Perturbation. IEEE Transactions on Neural Systems and Rehabilitation Engineering. 2010;18:461-7.
[18] Nikooyan AA, Zadpoor AA. Effects of Muscle Fatigue on the Ground Reaction Force and Soft-Tissue Vibrations During Running: A Model Study. IEEE Transactions on Biomedical Engineering. 2012;59:797-804.
[19] Pollock RD, Provan S, Martin FC, Newham DJ. The effects of whole body vibration on balance, joint position sense and cutaneous sensation. European journal of applied physiology. 2011;111:3069-77.
[20] Yang F, King GA, Dillon L, Su X. Controlled whole-body vibration training reduces risk of falls among community-dwelling older adults. Journal of biomechanics. 2015;48:3206-12.
[21] Kaeding TS, Moghaddamnia S, Kück M, Stein L. Deviations in frequency and mode of vibration in whole-body vibration training devices with long-term and regular use. Medical Engineering & Physics. 2018;51:84-90.
[22] Creaby MW, May K, Bennell KL. Insole effects on impact loading during walking. Ergonomics. 2011;54:665-71.
[23] Yoram F, Joseph W, Shay S, Reuven G. Attenuation of spinal transients at heel strike using viscoelastic heel insole: an in vivo study. Prev Med. 2004;39:351-4.
[24] Bruijn S, Meijer O, Beek P, Van Dieën J. Assessing the stability of human locomotion: a review of current measures. Journal of the Royal Society Interface. 2013;10:20120999.
[25] Simon AL, Ilharreborde B, Souchet P, Kaufman KR. Dynamic balance assessment during gait in spinal pathologies - a literature review. Orthopaedics & traumatology, surgery & research : OTSR. 2015;101:235-46.
[26] Ardestani MM, ZhenXian C, Noori H, Moazen M, Jin Z. Computational Analysis of Knee Joint Stability Following Total Knee Arthroplasty. Journal of Biomechanics. 2019.
[27] Morgan KD, Donnelly CJ, Reinbolt JA. Empirical Based Modeling for the Assessment of Dynamic Knee Stability: Implications for Anterior Cruciate Ligament Injury Risk. 2018 40th Annual International Conference of the IEEE Engineering in Medicine and Biology Society (EMBC)2018. p. 1676-9.
[28] Morgan KD, Zheng Y, Bush H, Noehren B. Nyquist and Bode stability criteria to assess changes in dynamic knee stability in healthy and anterior cruciate ligament reconstructed individuals during walking. Journal of Biomechanics. 2016;49:1686-91.
[29] Neptune R, Vistamehr A. Dynamic Balance during Human Movement: Measurement and Control Mechanisms. Journal of Biomechanical Engineering. 2018.
[30] Choi H, Peters KM, MacConnell MB, Ly KK, Eckert ES, Steele KM. Impact of ankle foot orthosis stiffness on Achilles tendon and gastrocnemius function during unimpaired gait. Journal of biomechanics. 2017;64:145-52.
[31] Huang T-wP, Kuo AD. Mechanics and energetics of load carriage during human walking. The Journal of Experimental Biology. 2014;217:605-13.
[32] Ultraflex. https://orthoactive.com/product/6841-ultraflex-uss-adult-afo-joint/. 2018.
[33] Totah D, Menon M, Jones-Hershinow C, Barton K, Gates DH. The impact of ankle-foot orthosis stiffness on gait: A systematic literature review. Gait & Posture. 2019;69:101-11.

[34] C-Motion_Markers. https://www.c-motion.com/v3dwiki/index.php/Marker_Set_Guidelines#Model_1. 2019.
[35] Chen C-J, Chou L-S. Center of mass position relative to the ankle during walking: A clinically feasible detection method for gait imbalance. Gait & Posture. 2010;31:391-3.
[36] Lugade V, Lin V, Chou L-S. Center of mass and base of support interaction during gait. Gait & posture. 2011;33:406-11.
[37] Mahmood I, Martinez-Hernandez U, Dehghani-Sanij AA. Evaluation of gait transitional phases using neuromechanical outputs and somatosensory inputs in an overground walk. Human Movement Science. 2020;69:102558.
[38] Blum KP, Lamotte D'Incamps B, Zytnicki D, Ting LH. Force encoding in muscle spindles during stretch of passive muscle. PLOS Computational Biology. 2017;13:e1005767.
[39] Rabuffetti M, Bovi G, Quadri PL, Cattaneo D, Benvenuti F, Ferrarin M. An experimental paradigm to assess postural stabilization: no more movement and not yet posture. IEEE Transactions on Neural Systems and Rehabilitation Engineering. 2011;19:420-6.
[40] Rakheja S, Dong RG, Patra S, Boileau PÉ, Marcotte P, Warren C. Biodynamics of the human body under whole-body vibration: Synthesis of the reported data. International Journal of Industrial Ergonomics. 2010;40:710-32.
[41] Sinclair J, Taylor PJ, Hobbs SJ. Digital filtering of three-dimensional lower extremity kinematics: an assessment. J Hum Kinet. 2013;39:25-36.
[42] Kulmala J-P, Korhonen MT, Kuitunen S, Suominen H, Heinonen A, Mikkola A, et al. Which muscles compromise human locomotor performance with age? Journal of The Royal Society Interface. 2014;11:20140858.
[43] Bizovska L, Svoboda Z, Kutilek P, Janura M, Gaba A, Kovacikova Z. Variability of centre of pressure movement during gait in young and middle-aged women. Gait & Posture. 2014;40:399-402.
[44] Anderson SR, Porrill J, Sklavos S, Gandhi NJ, Sparks DL, Dean P. Dynamics of Primate Oculomotor Plant Revealed by Effects of Abducens Microstimulation. Journal of Neurophysiology. 2009;101:2907-23.
[45] Sklavos S, Porrill J, Kaneko CRS, Dean P. Evidence for wide range of time scales in oculomotor plant dynamics: Implications for models of eye-movement control. Vision Research. 2005;45:1525-42.
[46] Maslivec A, Bampouras TM, Dewhurst S, Vannozzi G, Macaluso A, Laudani L. Mechanisms of head stability during gait initiation in young and older women: A neuro-mechanical analysis. Journal of Electromyography and Kinesiology. 2018;38:103-10.
[47] Pratt J, Krupp B, Morse C. Series elastic actuators for high fidelity force control. Industrial Robot: An International Journal. 2002;29:234-41.
[48] Toosi YB. A Note on the Gain and Phase Margin Concepts. Journal of Control and Systems Engineering. 2015;3:51-9.
[49] Benjamin C. Kuo FG. Automatic Control Systems. 9 ed: Prentice Hall PTR; 2003.
[50] Nigg BM. The role of impact forces and foot pronation: a new paradigm. Clinical journal of sport medicine : official journal of the Canadian Academy of Sport Medicine. 2001;11:2-9.
[51] Schut IM, Engelhart D, Pasma JH, Aarts RGKM, Schouten AC. Compliant support surfaces affect sensory reweighting during balance control. Gait & Posture. 2017;53:241-7.
[52] Coghe G, Pau M, Mamusa E, Pisano C, Corona F, Pilloni G, et al. Quantifying gait impairment in individuals affected by Charcot-Marie-Tooth disease: the usefulness of gait profile score and gait variable score. Disability and Rehabilitation. 2018:1-6.

Table 1

Table 1. The ankle-foot restricted conditions simulated using an adjustable ankle-foot orthosis (AFO).

AFO Restrictions (Single limb)	Abbreviation	Range
Normal (without AFO)	Normal	-
AFO restriction free	AFO (reference)	Free
Dorsiflexion resistive torque	DRT	33Nm
Dorsiflexion range-of-motion restriction	DRR	35°±5°
Dorsi-plantarflexion resistive torques	DPRT	±33Nm
Dorsi-plantarflexion range-of-motion restrictions	DPRR	±35°±5°

Figure 1

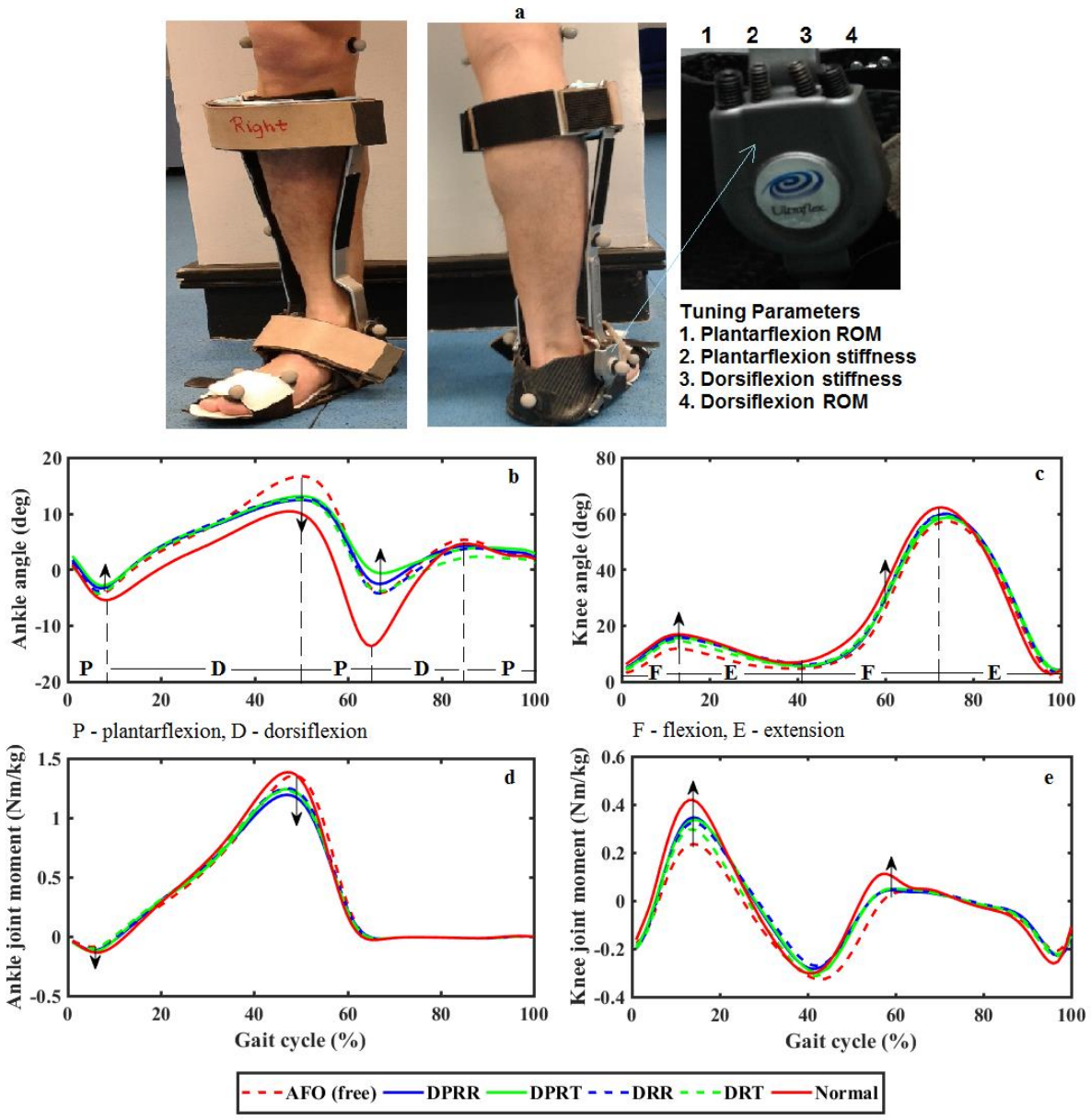

Figure 1. Ankle-foot orthosis and resultant ankle and knee joints angle and moment waveforms are plotted for with/without AFO restrictions.

650 **Figure 2**

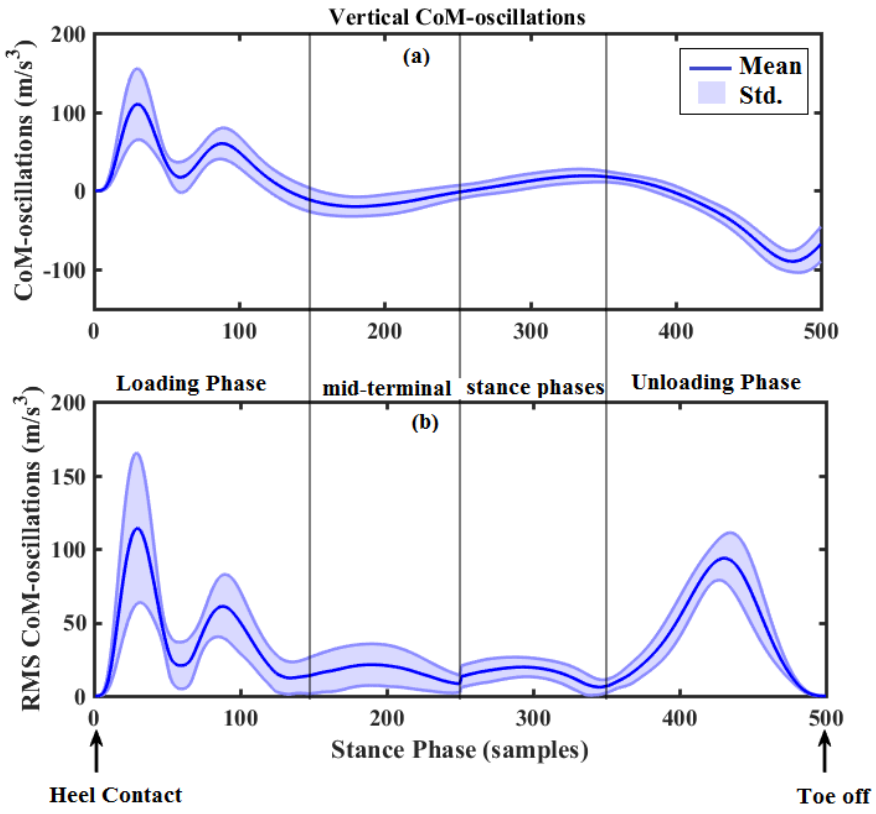

651

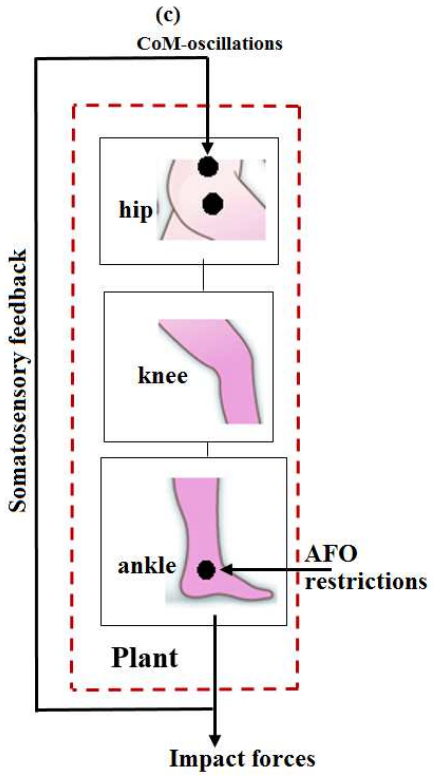

652

653 Figure 2. Rate of change in vertical-GRF illustrating impulsive oscillations during loading and
654 unloading of stance phase. (a) actual CoM-oscillations, (b) root-mean-square (RMS) values of CoM-
655 oscillations, (c) CoM-oscillations act as somatosensory feedback.

Figure 3

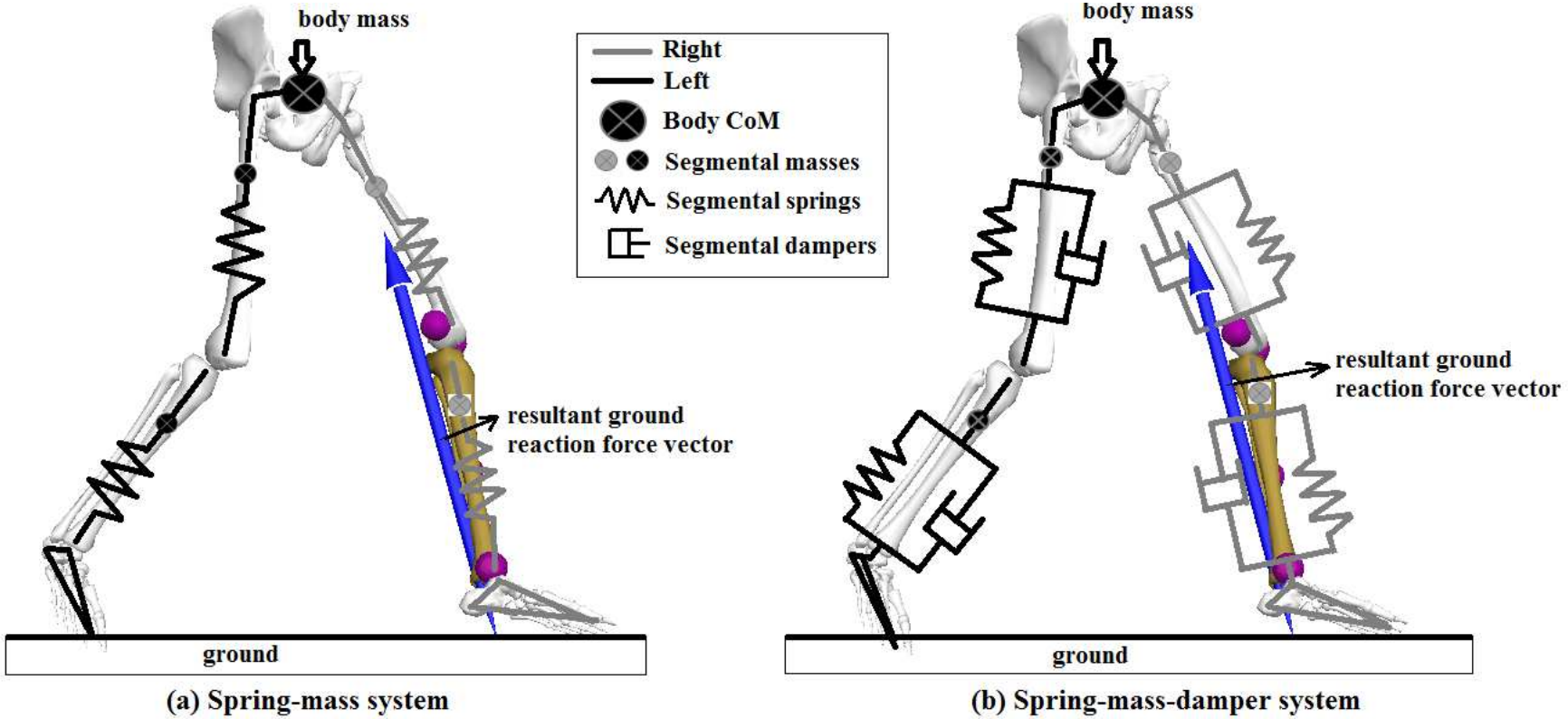

Figure 3. Lower limb model identification approaches using vertical-GRF. (a) Spring-mass (SM) model, (b) Spring-mass-damper (SMD) model.

Figure 4

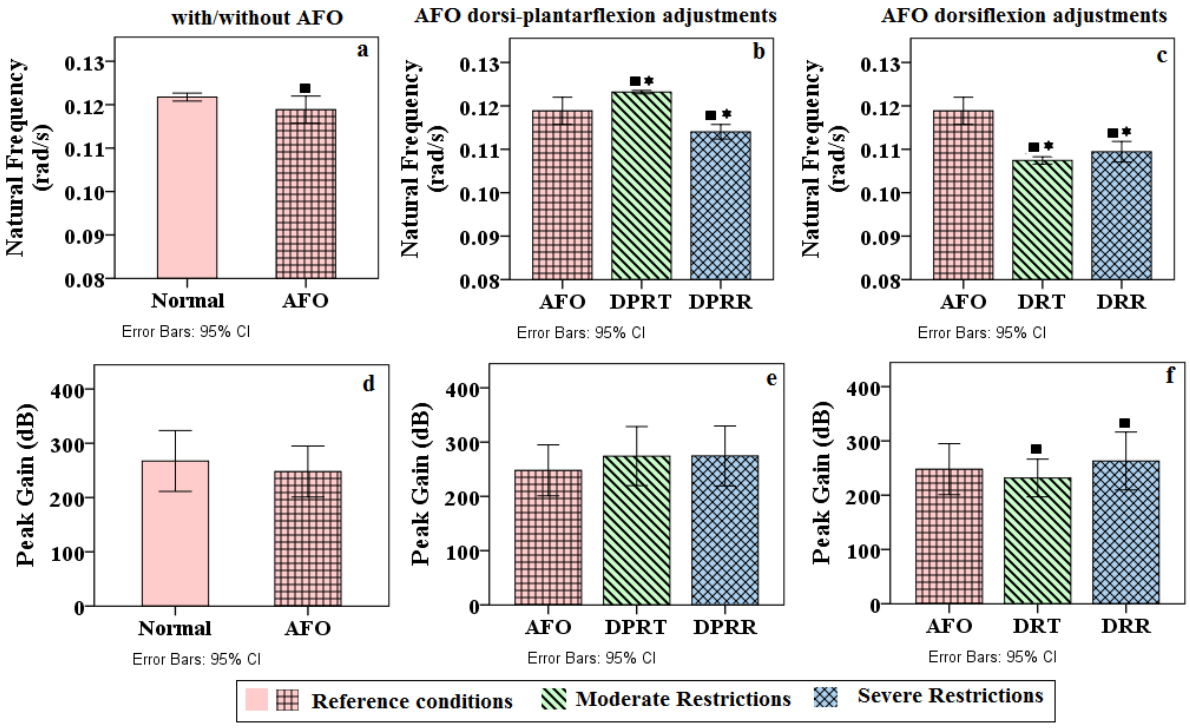

Figure 4. Lower limb contractile dynamics quantified from loading impact using a spring-mass model identification approach. '★' illustrate a significant difference with a normal walk, '■' illustrate the significant difference with an AFO free-mode walk.

Figure 5

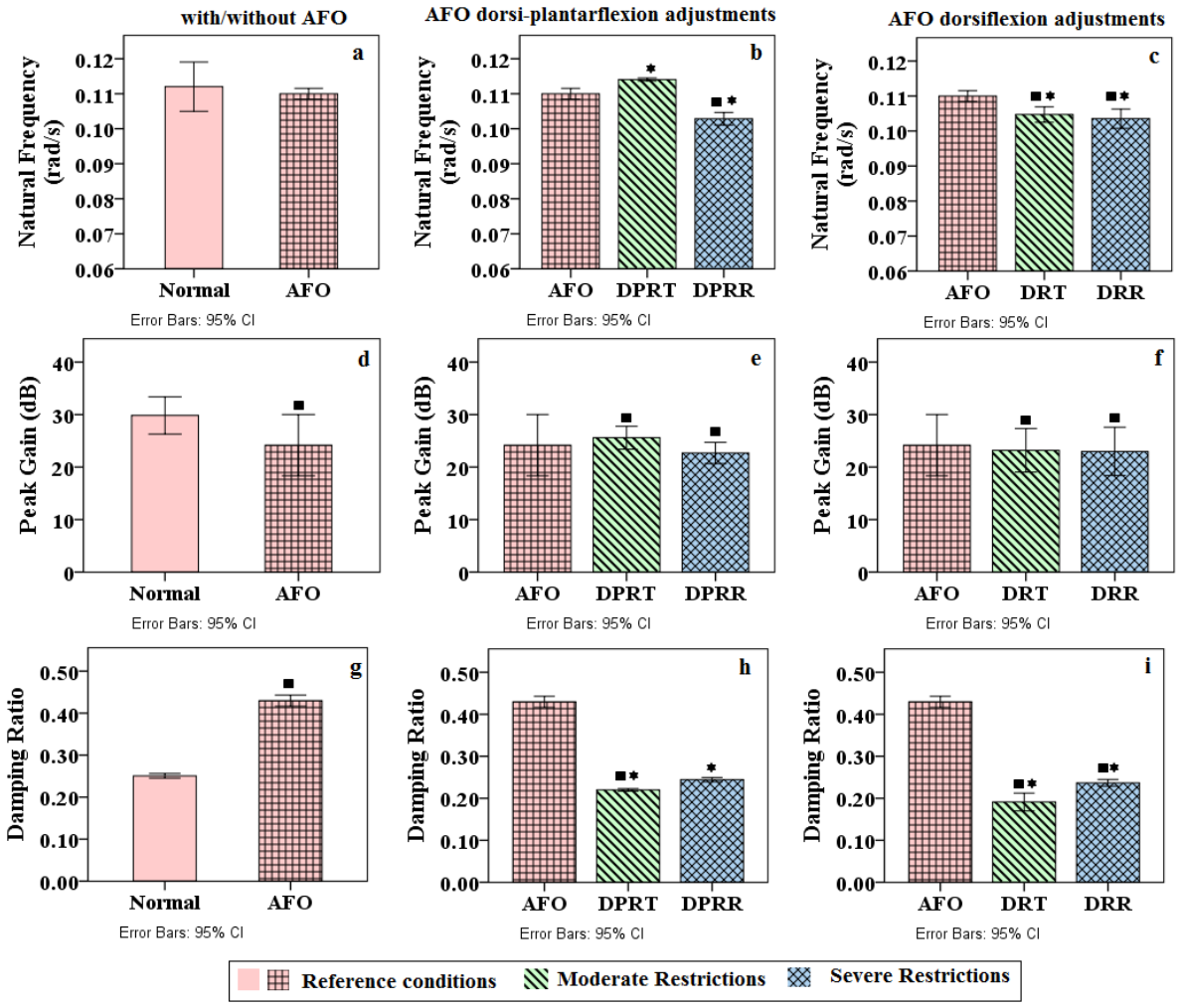

Figure 5. Lower limb contractile dynamics quantified from loading impact using spring-mass-damper model identification approach. '★' illustrate a significant difference with a normal walk, '■' illustrate the significant difference with an AFO free-mode walk.

Figure 6

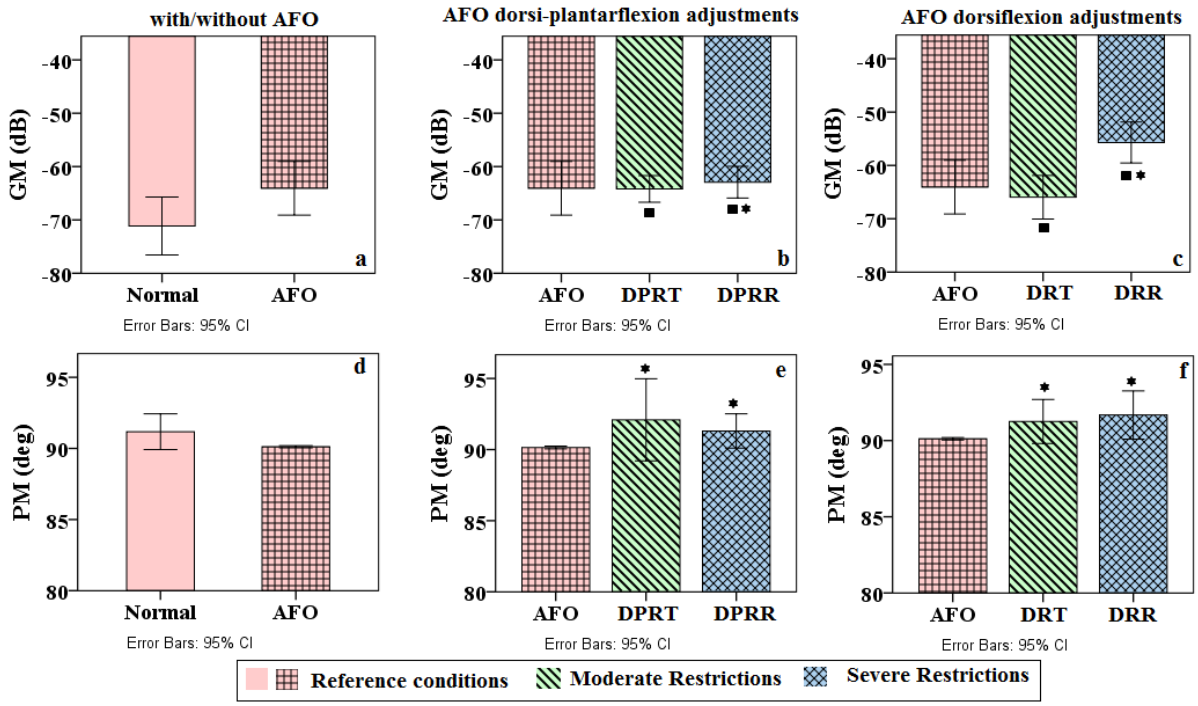

Figure 6. Loading phases stability margins compared to gain margins (GM) and phase margins (PM) with and without the effect of an ankle-foot orthosis (AFO). '★' illustrate a significant difference with a normal walk, '■' illustrate a significant difference with an AFO free-mode walk.

Figure 7

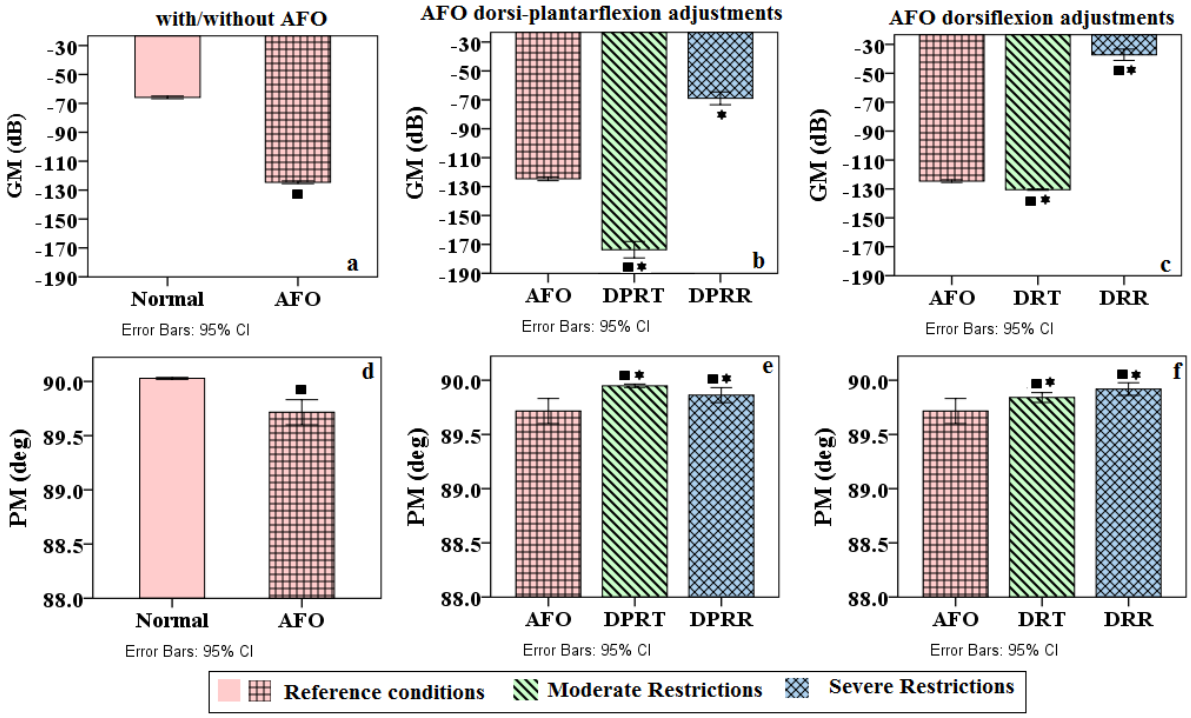

Figure 7. Unloading phases stability margins compared with and without an ankle-foot orthosis (AFO). '★' illustrate a significant difference with a normal walk, '■' illustrate a significant difference with an AFO free-mode walk.